J. Fluid Mech. (1999), *vol.* 388, *pp.* 197–215. Printed in the United Kingdom

Weak convection, liquid inclusions and the formation of chimneys in mushy layers

By T. P. SCHULZE[1] AND M. GRAE WORSTER[2]

[1] Courant Institute of Mathematical Sciences, New York University, 251 Mercer St., New York, NY 10012, USA
[2] Institute of Theoretical Geophysics, Department of Applied Mathematics and Theoretical Physics, University of Cambridge, Silver Street, Cambridge CB3 9EW, UK

(Received 10 June 1998 and in revised form 2 January 1999)

We present a numerical study of steady convection in a two-dimensional mushy layer during solidification of a binary mixture at a constant speed V. The mushy layer is modelled as a reactive porous medium whose permeability is a function of the local solid fraction. The flow in the liquid region above the mushy layer is modelled using the Stokes equations (i.e. the Prandtl number is taken to be infinite). The calculations follow the development of buoyancy-driven convection as the flow amplitude is increased to the level where the solid fraction is driven to zero at some point within the mushy region. We show that this event cannot occur before the local buoyancy-driven volume flux exceeds the solidification rate V. Further increases in the flow amplitude lead to the formation of a region with negative solid fraction, indicating the need to switch from the Darcy approximation to the Stokes flow approximation. These regions ultimately become what are known as chimneys. We exhibit solutions which give the detailed structure of the temperature, solute, flow and solid fraction fields within the mushy layer. A key finding of the numerics is that these fledgling chimneys emerge from the interior of the mushy layer, rather than eating their way down from the top of the layer, as the amplitude of the steady convection is increased. We discuss some qualitative features of the resulting liquid inclusions and, in the light of these, reassess the interfacial conditions between mushy and liquid regions.

1. Introduction

The term 'mushy layer' refers to the interfacial region between solid and liquid in the case where this interface has become dendritic as the result of a morphological instability. There is an extensive literature investigating the details of this instability (see review by Coriell & McFadden 1993); our focus here is on convective processes that take place within the mushy layer on length scales much greater than the dendrite spacing.

Mushy layers are prevalent during the solidification of metallic alloys, magmas and aqueous solutions. Even pure materials can lead to the formation of mushy layers, provided the liquid is cooled to a meta-stable state below its melting temperature. Of particular interest in these systems is the formation of 'chimneys', which are narrow, dendrite-free, cylindrical regions that form within the mushy layer as the result of convection. This striking phenomenon is known to occur within solidifying alloys (Hellawell, Sarazin & Steube 1993), where it is responsible for undesirable material

properties; within sea ice (Eide & Martin 1975), where it has a significant effect on ocean dynamics; within magma chambers (Tait & Jaupart 1992), where it influences mineral deposits, and it may occur at the Earth's inner–outer core boundary (Fearn, Loper & Roberts 1981; Bergman & Fearn 1994).

Ironically, the mechanisms behind the dissolution of dendrites within the chimney are the same as those responsible for the formation of the dendrites in the first place. The initial instability begins with solute being rejected at the interface†, resulting in a compositional boundary layer. The melting temperature of the alloy is a function of the solute concentration and increases in the direction of the liquid as a result of this boundary layer, promoting the continued growth of interfacial perturbations. The mushy layer is a strongly nonlinear manifestation of this instability. If the rejected material's density is less (more) than that of the bulk fluid and the material is being cooled from below (above), solute rejection can also lead to a convective instability. When the convection is sufficiently strong, the solute-rich material that flows out of the mushy layer locally depresses the melting temperature, redissolving some of the dendrites. The enhanced permeability in these dissolved regions causes the focusing of the outflow into plumes.

The evolution of individual dendrites is notoriously difficult to compute. To study the macro-scale dynamics of the convection, however, we follow the example of many previous studies (see Beckermann & Wang 1995 and Worster 1997 for extensive reviews) and treat the mushy layer as a porous medium with physical properties that are volume-fraction-weighted averages of the liquid and solid properties. We model fluid flow within the mushy layer using Darcy's equation with a solid-fraction-dependent permeability and pose boundary conditions at the mush–liquid interface. The local solid fraction (averaged over the inter-dendritic scale) is determined by applying a condition of local thermodynamic equilibrium, which is assumed to apply on small scales as a result of the intimate contact between liquid and solid.

Such models are well established in the literature, having grown out of the work of Flemings and co-workers (e.g. Flemings & Nereo 1967,1968) and given a thermodynamic foundation by Hills, Loper & Roberts (1983). Recent work in this area seems to have bifurcated into two distinct groups. For the most part, computational work has used a Darcy–Brinkman formulation of the problem, which seeks to use a single momentum equation for both the liquid and mushy phases. This work (see Beckermann & Wang 1995 for review) is aimed at metallurgical studies that follow the time-dependent evolution of castings using detailed models that look for quantitative prediction of a casting's composition as a function of depth. Chimneys are readily observed in this type of study, although they are not highly resolved and have not generally been the focus of these studies.

A second group has focused on the linear (Fowler 1985; Worster 1992; Chen, Lu & Yang 1994; Anderson & Worster 1995*b*) and weakly nonlinear (Amberg & Homsy 1993; Anderson & Worster 1995*a*) convective instability using a variety of simplifications and favouring a free-boundary formulation involving distinct equations in the liquid (Navier–Stokes equation) and mushy (Darcy's equation) regions. Chimneys are only present in spirit in these studies, in that there is a reduction in the solid fraction in the upflowing regions of a convection cell.

Building on an early model for fully developed chimneys put forward by Roberts & Loper (1983), Schulze & Worster (1998) sought to push this latter type of study

† Here we mean the term 'solute rejection' to include cases, like solidifying ammonium-chloride solutions, where water is the rejected material.

into the fully nonlinear regime by performing computations using the porous-medium model within a two-dimensional mushy layer that was punctured at periodic intervals by narrow chimneys. The flow in chimneys was modelled using lubrication theory and other approximations. This work falls short of completely resolved chimneys in that the free boundaries were treated in an *ad hoc* manner that maintained a rectangular computational geometry.

The present study continues to work in a two-dimensional setting and seeks to bridge the gap between the weakly nonlinear theories and the numerical work of Schulze & Worster (1998). It improves on the latter work by resolving the free boundary between the mushy and liquid regions and solving the equations in the liquid region using a Stokes flow approximation. It is less ambitious in that it stops short of featuring fully developed chimneys. Instead, it extends the weakly nonlinear studies in that it relaxes assumptions, like a fixed, flat, impermeable mush–liquid boundary, that were used to facilitate analytical progress. The development of steady-state convection can be followed from onset to the first appearance of negative solid fraction within the mushy layer. This corresponds to the conception of chimneys as one moves along the continuum of steady states in the direction of increasing flow amplitude. The bifurcation is subcritical, so that these solutions are unstable, requiring the use of a continuation algorithm to achieve convergence of the numerical scheme. This work is most similar to the work of Emms (1998), which analyses time-evolving convection in a mushy layer with fixed permeability.

Below, we present the equations and boundary conditions (§ 2), describe the numerical methods (§ 3), present some computational results (§ 4) and discuss the results and their relationship to previous work (§ 5). In § 6 we extend the discussion to include an itemization of what boundary conditions are necessary to resolve liquid inclusions and outline some of the qualitative features that characterize such solutions.

2. Formulation

Consider the physical domain consisting of a horizontal mushy layer sandwiched between semi-infinite liquid and solid layers (figure 1). A steady state with this geometry can be established by forcing liquid at constant speed through a temperature gradient that is fixed in the laboratory frame of reference. We emphasize that while the solid–mush and mush–liquid interfaces are stationary in this frame of reference, the solid formed at the base of the mushy layer and the solid structure within the mushy layer are moving down at uniform speed with respect to these interfaces. The convective flows that form within the liquid and mushy layer bifurcate from this uniform downflow.

This crystal-pulling configuration is in contrast to solidification configurations where the interfaces move away from a stationary boundary which is held at a fixed temperature (metal chilling in a crucible, for example.) In these latter cases, the interfaces slow down as they get further from the boundary and the system is always in a transient state. The difference between these two formulations of the problem marks another significant difference between previous analytical work and the bulk of the numerical work, as the steady-state formulation is preferable for studies focusing on stability and bifurcation.

Our model features the following additional assumptions: Darcy flow in the mushy layer with solid-fraction-dependent permeability; Stokes flow in the liquid region (infinite Prandtl number); neglect of solutal diffusivity in both regions; neglect of thermal buoyancy; local thermodynamic equilibrium in the mushy layer; equal thermal prop-

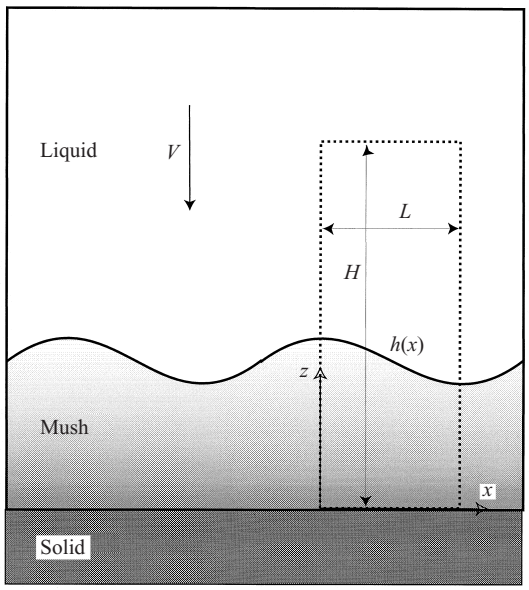

FIGURE 1. Definition sketch of the system under consideration, showing the solid, mushy layer, liquid and plume.

erties in liquid and solid phases; no change in density upon solidification; complete solute rejection. Most of these are discussed in Worster (1997) and/or Schulze & Worster (1998).

Using this idealized model, one can scale the temperature and concentration so that, within the mushy region, they are equal to one another:

$$\theta = [T - T_L(C_0)]\,/\Delta T = (C - C_0)/\Delta C. \tag{2.1}$$

Here $\Delta T = \Gamma\,\Delta C = T_L(C_0) - T_E$ is the difference between the liquidus (freezing) temperature at the far-field concentration and the eutectic temperature, $\Delta C = C_0 - C_E$ is the difference between the far-field concentration and the eutectic concentration and Γ is the slope of the liquidus. The same scaling and reference value are used for the bulk concentration $\bar{C}$, defined below. We use the symbol $\boldsymbol{u}$ for both the fluid velocity in the liquid region and the volume flux of fluid per unit area in the mushy region and non-dimensionalize these with the vertical pulling speed (solidification rate) V. Distance is scaled with the thermal diffusion length scale κ/V and permeability with a characteristic value Π_0.

The governing equations in the bulk of the mushy region are given by conservation of heat and solute, the relationship between the bulk ($\bar{C}$) and interstitial (θ) concentration, the curl of Darcy's equation recast in terms of a stream function ψ, and a function relating permeability to the local solid fraction ϕ:

$$\nabla^2\theta + \theta_z = \boldsymbol{u}\cdot\nabla\theta + S\phi_z, \tag{2.2a}$$

$$\bar{C}_z = \boldsymbol{u}\cdot\nabla\theta, \tag{2.2b}$$

$$\bar{C} = (1-\phi)\theta + \mathscr{C}\phi, \tag{2.2c}$$

$$\nabla^2\psi = -Ra\,\Pi\,\theta_x + (\nabla\Pi\cdot\nabla\psi)/\Pi, \tag{2.2d}$$

$$\Pi = (1-\phi)^3. \tag{2.2e}$$

Here the stream function is defined by the relationship $\boldsymbol{u} = \{-\psi_z, \psi_x\} = \nabla \times (\psi \hat{\boldsymbol{j}})$ and the Lewis number $Le = \kappa/D$ has been set to infinity. The presence of the θ_z and $\bar{C}_z$ terms in equations (2.2*a*, *b*) result from the decomposition of the vertical volume flux into a portion (scaled to unity) due to the vertical pulling speed and a buoyancy-driven portion w. The left-hand side of equation (2.2*b*) then represents the advection of the solute in both the solid dendrites and the interstitial fluid by the vertical pulling speed; the right-hand side of the equation represents the advection of the interstitial fluid by the buoyancy-driven portion of the flow. Equation (2.2*e*) is a commonly used empirical relationship; see Worster 1992 for a discussion of alternatives. The exponent in this power law may vary depending on the permeability structure of the material under consideration, but the essential feature of this relationship is that the permeability is a decreasing function of solid fraction. Note that this contributes to the focusing of upflow and the formation of chimneys (Amberg & Homsy 1993).

The non-dimensional variables in these equations are the Stefan number S, a concentration ratio $\mathscr{C}$ and the solutal porous-medium Rayleigh number Ra:

$$S = \frac{\mathscr{L}}{c\Delta T}, \quad \mathscr{C} = \frac{C_S - C_0}{\Delta C}, \quad Ra = \frac{\beta \Delta C g \Pi_0}{\nu V}, \tag{2.3}$$

where $\mathscr{L}$ is the latent heat of fusion, c is the specific heat, β is the solutal expansion coefficient, g is the acceleration due to gravity, ν is the kinematic viscosity and C_S is the concentration of the solid phase.

In the liquid region, the solid fraction is zero and the temperature and concentration are unconstrained by the liquidus relationship. We take the Prandtl number ν/κ to be infinite, so that we have Stokes flow in the liquid region. While one can one can justify this approximation for aqueous solutions, magmas and other highly viscous materials, this is done primarily for convenience. The governing equations are conservation of heat and solute, along with the Stokes equations, which we write in terms of the stream function and the component of vorticity oriented perpendicular to the (x, z)-plane ($\omega \hat{\boldsymbol{j}} = \nabla \times \boldsymbol{u}$):

$$\nabla^2 T + T_z = \boldsymbol{u} \cdot \nabla T, \tag{2.4a}$$

$$C_z = \boldsymbol{u} \cdot \nabla C, \tag{2.4b}$$

$$\nabla^2 \omega = -\frac{Ra}{Da} C_x, \tag{2.4c}$$

$$\nabla^2 \psi = -\omega. \tag{2.4d}$$

The Darcy number $Da = \Pi_0 V^2/\kappa^2$ is the ratio of the permeability scale to the square of the thermal-diffusion length scale (on which the macroscopic dimensions of the mushy layer scale), and must be small for the porous medium assumption to hold.

Prior to plume formation, boundary conditions on the exterior of the computational domain are straightforward. At the top of the liquid region, we specify uniform downflow consistent with the pulling speed V; temperature and concentration are prescribed at the (scaled) far-field values T_0 and zero, respectively. At the bottom of the mushy layer, temperature and concentration are equal to their eutectic values, so that this interface is flat. The fluid passing through the lower boundary and becoming solid must once again move downward with the uniform pulling speed. Finally, we

pose symmetry conditions in order to isolate a single convection cell:

$$\psi = \omega = C = 0,\ T = T_0 \quad \text{at} \quad z = H, \tag{2.5a}$$

$$\psi = 0,\ \theta = -1 \quad \text{at} \quad z = 0, \tag{2.5b}$$

$$\psi = \theta_x = 0 \quad \text{at} \quad x = 0, L, \quad z < h(x), \tag{2.5c}$$

$$\psi = \psi_{xx} = \theta_x = C_x = 0 \quad \text{at} \quad x = 0, L, \quad z > h(x), \tag{2.5d}$$

where L and H are the (scaled) horizontal and vertical dimensions of the computational domain and $h(x)$ is the position of the mush–liquid interface, figure 1.

At the mush–liquid interface (whether it be freezing or dissolving), one must have continuity of pressure, mass flux and temperature. Along freezing interfaces, one must pose a boundary condition that defines the envelope of the dendritic region. Worster (1986) shows that the condition $\phi = 0$ is often consistent with a more general condition of 'marginal equilibrium', which is based on the notion that there should be no constitutional supercooling on the liquid side of the interface (i.e. the temperature should be at or above the liquidus temperature throughout the liquid region if the assumption of local thermodynamic equilibrium is to be enforced). In cases where the solid fraction can be taken to be zero, conservation of heat and solute then require continuity of the temperature gradient and concentration. If the solid fraction at the interface is non-zero, there are discontinuities in these quantities, owing to the production of latent heat and solute rejection. This can happen when there are differences in the thermal properties of the mush and liquid or in the limit of vanishing solutal diffusivity. In the latter case, which we consider here, the nature of the boundary conditions that govern the concentration, solid fraction and interface position depends on the direction of flow. We postpone a general discussion of these boundary conditions to § 6, where we consider some qualitative features of mushy layers containing liquid inclusions and the formation of chimneys. When the mushy layer is free of these features, the flow is always from liquid to mush along a freezing interface. In this case, which is the only one encountered in our computations, local equilibrium can be enforced by simply extending the liquidus constraint to the liquid side of the interface. This ensures continuity of the solute concentration and forces the solid fraction to be zero.

In the absence of solutal diffusivity, solute is passively advected along streamlines so that the concentration at the interface is equal to that in the far field (which we have scaled to zero) wherever streamlines flow into the mushy layer. Combining this result with the liquidus constraint provides us with the interfacial temperature. A final simplification can be achieved by taking advantage of the smallness of the Darcy number. This greatly increases the effective Rayleigh number in the liquid region, so that there is an approximate balance between pressure and buoyancy, implying little variation in pressure along isopycnals (Emms & Fowler 1984).

The considerations outlined above lead to a remarkably simple set of interfacial conditions:

$$[\psi]^l_m = p = [\hat{\boldsymbol{n}} \cdot \nabla T]^l_m = T = C = \theta = \phi = 0 \quad \text{at} \quad z = h(x), \tag{2.6}$$

where the l- and m-super/subscripts indicate the change in the bracketed quantities across the interface.

We require one more condition on the liquid side of the interface since the flow there is governed by a fourth-order, rather than second-order, operator. One possibility is

to apply the Beavers–Joseph condition (Beavers & Joseph 1967):

$$[\boldsymbol{u}\cdot\hat{\boldsymbol{t}}]_l^m = \alpha Da^{1/2}\hat{\boldsymbol{n}}\cdot\nabla\boldsymbol{u}, \tag{2.7}$$

where $\hat{\boldsymbol{t}}$ is a unit vector tangent to the interface and α is an empirically determined non-dimensional material parameter, which we assume to be $O(1)$. The smallness of the Darcy number then implies that the tangential component of the fluid velocity is continuous, to a first approximation, at all mush–liquid interfaces. An alternative to (2.7) is to apply a no-slip condition, so that the tangential component of the fluid velocity matches that of the uniformly translating dendrites:

$$\boldsymbol{u}\cdot\hat{\boldsymbol{t}} = 0. \tag{2.8}$$

Darcy's equation can be used to show that this condition applies on the mush side of the interface whenever $p = C = 0$ (see Schulze & Worster 1998), ensuring the continuity of both the tangential and normal components of the velocity across the interface. Thus, for the computations presented in §§ 3–5, where the mush–liquid interface is an isopycnal, (2.7) and (2.8) are equivalent. Along the more general interfaces discussed in § 6, however, (2.8) can lead to discontinuities in the tangential component of the velocity. When considering the thermodynamic relationships at the interface, it seems more appropriate to adopt (2.7).

3. Computational procedures

Before solving the equations (2.2) and (2.4) we employ a transformation to map the free-boundary problem to a fixed domain. We use separate transformations in the mushy and liquid regions, so that each is mapped to a rectangular region with vertical coordinate ranging from zero to one:

$$\xi_m = x_m, \qquad \zeta_m = \frac{z_m}{h}, \tag{3.1a}$$

$$\xi_l = x_l, \quad \zeta_l = \frac{z_l - h}{H - h}. \tag{3.1b}$$

The x-coordinate is unchanged by this transformation, but derivatives with respect to both x and z are affected:

$$\frac{\partial}{\partial x_m} = \frac{\partial}{\partial \xi_m} - \frac{\zeta_m}{h}\frac{\partial h}{\partial \xi_m}\frac{\partial}{\partial \zeta_m}, \tag{3.2a}$$

$$\frac{\partial}{\partial z_m} = \frac{1}{h}\frac{\partial}{\partial \zeta_m}, \tag{3.2b}$$

$$\frac{\partial}{\partial x_l} = \frac{\partial}{\partial \xi_l} - \frac{1-\zeta_l}{H-h}\frac{\partial h}{\partial \xi_l}\frac{\partial}{\partial \zeta_l}, \tag{3.2c}$$

$$\frac{\partial}{\partial z_l} = \frac{1}{H-h}\frac{\partial}{\partial \zeta_l}. \tag{3.2d}$$

Second derivatives follow from the chain rule.

We use second-order-accurate difference formulas for the ξ- and ζ-derivatives, and implement equations (3.2*a–d*) via subroutines that switch from centred differences to differences biased away from boundaries at the edge of the computational domain. All of the figures in this text were computed using 32×32 grid points per one-

half of a convection cell. Mesh refinement was used to verify accuracy for selected computations.

The basic method employed to solve the governing equations is iteration with successive over-relaxation. The elliptic operators in equations (2.2) and (2.4) are iterated using Gauss–Seidel iteration (Press *et al*. 1992), with the nonlinear terms, including those introduced by the transformations (3.1), evaluated simultaneously, using data from the previous iteration. The bulk concentration is determined using a simple quadrature of equation (2.2*b*), which then allows one to update the solid fraction using (2.2*c*) and the permeability using (2.2*e*). Equation (2.4*b*) has the solution $C = 0$ prior to chimney and plume formation, which is the case we consider here. The interface position is updated using the boundary condition (2.6*c*), the transformations (3.1) having explicitly introduced $h(\xi)$ into this relationship. We seek steady convective solutions for a half-cell of a periodically extended system by continuing the iteration until there are no appreciable changes. The iteration scheme is, however, inherently time-like, and it is necessary to employ a continuation scheme in order to converge to unstable solutions.

The first step in the continuation scheme is to predict a new solution using a linear extrapolation of previously computed solutions. During the subsequent iteration of this predicted solution, the stream function (or some other flow quantity) at a specified grid point is held at its predicted value. This prevents the scheme from drifting away from unstable solutions. To do this, one must relax some other constraint on the system or it will be over-determined. We choose the Rayleigh number for this purpose, and use a root-finding scheme to determine a value for the Rayleigh number consistent with the predicted value of the stream function. This must be done once per iteration cycle, but involves solving only a single algebraic equation. One can think of this procedure as replacing the Rayleigh number with the flow amplitude in the set of parameters that identifies a particular steady solution.

For ease in locating the root, one should choose a grid point where the stream function is changing rapidly as one changes the Rayleigh number. It is easy to identify the grid point where the stream function varies most rapidly, but we found that this was not necessarily optimal. In fact, we frequently found that choosing the fastest varying grid point led to numerical instability. Since the flow structure was similar from one calculation to the next, we were able to determine regions of the flow that allowed for both rapid convergence and stability through experimentation. For the problem at hand, we had the best results with points that were somewhat below the centre of the mushy region.

When updating the remaining grid points using the iteration formula, we found it best to start the sweep with the grid point which was being held fixed. If one sweeps through the grid in some other fashion, it will be found that the coefficients in the equation solved to determine the Rayleigh number will have changed when the grid point at which the stream function is being held fixed is reached.

4. Computational results

Figure 2(*a*) shows the superimposed shapes of the interface for several levels of flow amplitude, starting with no convection (flat interface) and ending when the solid fraction has been driven down to zero at some point within the mush. The parameter values, which are given in the caption, are characteristic of experiments using ammonium-chloride solutions. The width of the computational domain was chosen to coincide with the linear critical wavelength.

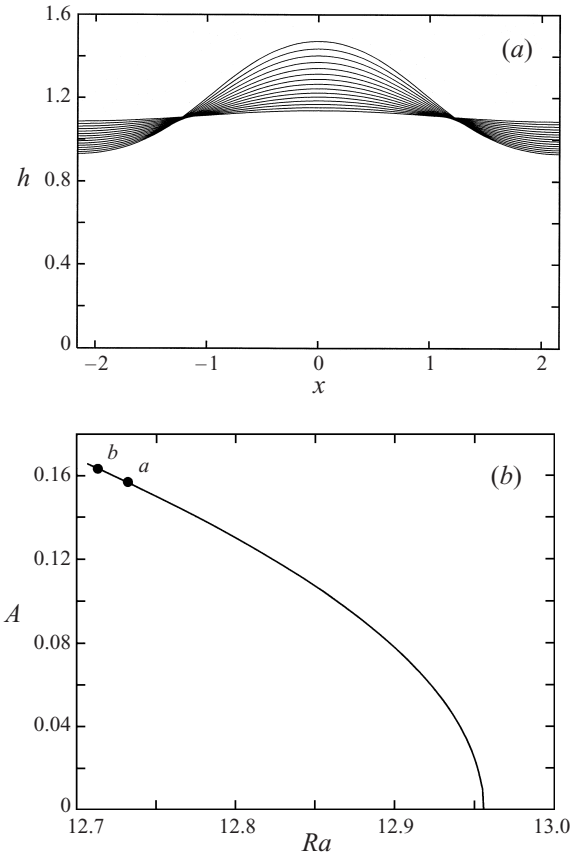

FIGURE 2. (*a*) The superimposed shapes of the interface for several levels of flow amplitude, starting with no convection (flat interface) and ending when the solid fraction has been driven below zero at some point within the mushy layer. The parameter values are characteristic of experiments with ammonium-chloride solutions: $\mathscr{C} = 15$, $S = 5$, $T_0 = 0.4$. We used $L = 2.16$ for the half-width of a convection cell, which corresponds to the linear critical wavelength for these parameter values. These solutions lie on the bifurcation diagram shown in (*b*), which gives the average value of the buoyancy-driven volume flux as a function of the Rayleigh number. The linear critical point corresponds to the flat interface in (*a*), while the points labelled *a* and *b* correspond to the solutions shown in figures 4(*a*) and 4(*b*).

In figure 2(*b*), these solutions are represented on a bifurcation diagram, where we plot flow amplitude versus Rayleigh number. For the chosen parameter values, we find that the bifurcation is sub-critical. This is consistent with the weakly nonlinear analysis of Amberg & Homsy (1993). The linear critical point is in agreement with the work of Worster (1992). As one would expect from a sub-critical pitchfork bifurcation, these solutions are unstable, necessitating the use of the continuation method described above.

It is worth emphasizing that although these solutions are weakly convecting in the sense that the convection has not become strong enough to overcome the downflow due to the pulling speed, no small-amplitude assumption has been made. Indeed, these weak flows are very different from those computed by the weakly nonlinear analysis, in that the interface undergoes significant up-welling at the centre of a convection cell. In contrast, all of the analytical solutions to date have featured flows confined

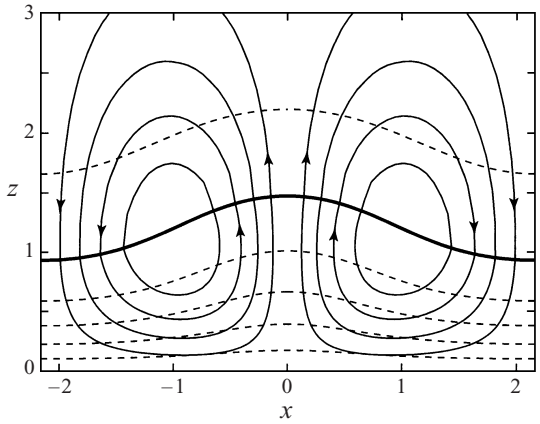

FIGURE 3. Flow information for a steady-state solution which has an amplitude just beyond the point at which the solid fraction has been driven to zero (point b on the bifurcation diagram shown in figure 2(b). The figure shows the interface, isotherms and streamlines for the buoyancy-driven portion of the volume flux. Recall that the interface is the $T = 0$ isotherm. The computational domain extends beyond that shown in the figure ($H = 10$).

to the mushy layer by a fixed, flat and *impermeable* mush–liquid interface. These assumptions were invoked to render the problem analytically more tractable but limit the validity of the results. For example, the latter studies do not quantitatively reproduce the linear stability results of Worster (1992), whereas the present study converges to those results as the mesh spacing is refined.

The up-welling of the interface is caused when buoyancy weakens the downflow in the centre of a convection cell, allowing the thermal boundary layer that bounds the mushy layer to expand. Direct experimental evidence for this effect is reported by Tait & Jaupart (1992). The up-welling is a weaker, less-focused version of the small volcano-shaped structures that are seen at chimney openings.

In figure 3 we plot detailed flow information for a steady-state solution which has a flow amplitude just beyond the point where the solid fraction has been driven to zero. The figure shows the interface, isotherms and streamlines for the buoyancy-driven portion of the volume flux. Examining the isotherms, which include the interface, we see further evidence for the expansion of the thermal boundary layer. The streamlines are reminiscent of the large-scale recirculation that takes place in conventional convection experiments, but we must keep in mind that the uniform downflow has been subtracted from the solution and that fluid particles do not follow these paths.

Figures 4(a)–4(b) show the interface, solid fraction contours and the streamlines for the total volume flux for solutions (a) just beyond the point where the total volume flux begins to recirculate and (b) just beyond the point where the solid fraction has become negative. Notice the closed zero-solid-fraction contour in the centre of (b). The solid fraction inside this contour is below zero, indicating that the mushy layer in this region should be replaced by a liquid inclusion. This represents the beginning of a nascent chimney, which will continue to develop with increasing flow amplitude until 'birth', when the inclusion breaks free of the mushy layer. Since these solutions are unstable for parameter values that characterize experiments, these embryonic states may not be physically observable. Such solutions are of interest, however, because they may give some insight into how chimneys form in a transient setting. There are

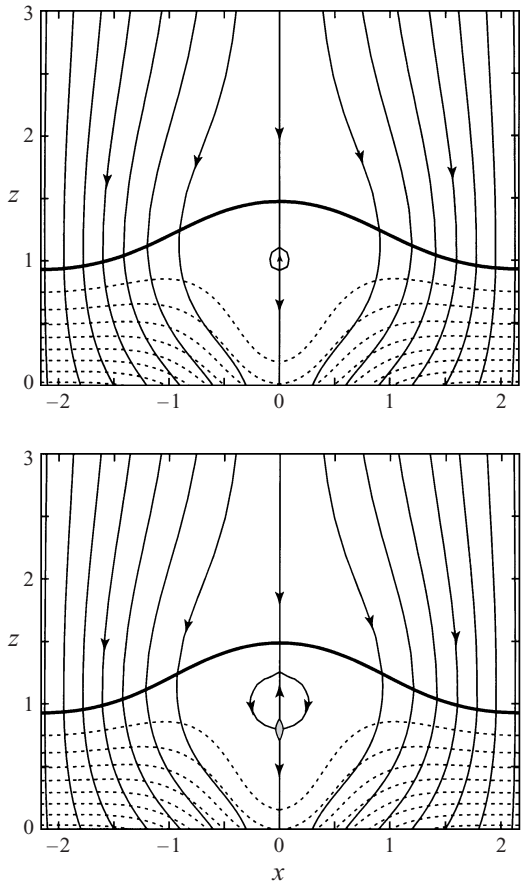

FIGURE 4. The interface, solid-fraction contours and the streamlines for the total volume flux for solutions (*a*) just beyond the point where the total volume flux begins to recirculate and (*b*) just beyond the point where the solid fraction has become negative – notice the closed zero-solid-fraction contour in the centre of (*b*). The solid fraction inside this contour is just below zero, indicating that the mushy layer in this region should be replaced by a fluid inclusion. The solid fraction contours range from 0 to 0.08; the parameter values are indicated in the caption for figure 2.

two features of these solutions that are especially interesting in this respect. First, the conception of the chimney is nearly coincident with the point where the buoyancy-driven volume flux is first equal to the volume flux due to the uniform pulling speed. Secondly, the chimney emerges from within the mushy layer rather than eating its way into the mushy layer from the top. An explanation for these features is given in the following section.

5. Discussion of computational results

The computations featured in the previous section suggest that chimneys begin to form internally rather than eating their way down from the top of the layer. This can be explained by the disparity in the thermal and solutal diffusivities, which causes the dissolution effects of the buoyant fluid to be more localized than the thermal effects. Thus, there is a cold boundary layer surrounding the dissolved region where solidification is actually enhanced, and this pushes the interface ahead of a developing

chimney. Note that this is the same effect that causes the build up of solid fraction in the thermal boundary layer surrounding a fully developed chimney (see Worster 1991 and Schulze & Worster 1998). To some extent, this also influences the up-welling of the interface, but this latter effect owes its existence more to the decreased flow rate and advective heat flux resulting from convection.

Our computations also show that chimneys do not form until the vertical component of the buoyancy-driven volume flux, w, exceeds the downward volume flux of both phases generated by the pulling speed. It has long been a metallurgical rule of thumb that chimneys form once the convective velocity exceeds the speed of the isotherms (Flemings 1974), a result also inferred from approximate analyses by Fowler (1985) and Tait & Jaupart (1992). Data from the present calculations show that while these two events are nearly coincident, w may exceed unity just before ϕ drops below zero (figure 5). We can see that these events must always occur in this order by examining equation (2.2b) with the bulk concentration replaced by (2.2c):

$$\theta_z - (\phi\theta)_z + \mathscr{C}\phi_z = \boldsymbol{u}\cdot\nabla\theta. \tag{5.1}$$

Along the vertical symmetry line where upflow first occurs, $u = 0$, and we may rewrite this equation as

$$\frac{\mathscr{C}-\theta}{\theta_z}\phi_z = \phi + Q, \tag{5.2}$$

where $Q = w - 1$ is the net volume flux in the upward direction. The coefficient multiplying the ϕ_z-term must be positive, since $\mathscr{C} > 0$, $\theta < 0$ and $\theta_z > 0$ for any physically reasonable system. This allows some insight into relationships that must hold for the Q- and ϕ-profiles along the symmetry line.

At the onset of convection, we know that the solid fraction is non-negative, monotonically decreasing and equal to zero only at the top of the mushy layer. As the strength of the convection increases, Q increases and ϕ decreases. Imagine viewing a continuous sequence of these profiles. After ϕ has dropped below zero at some height along this symmetry line, we know that the ϕ-profile must have a local minimum, since it decreases at the top of the mushy layer according to the arguments at the beginning of this section. Equation (5.2) tells us that the signs of Q and ϕ must disagree at this local minimum, so that the net volume flux must have become positive no later than the time when ϕ first became negative. These events coincide if ϕ and ϕ_z first become zero at the same time.

Our computations indicate that a positive volume flux is achieved just before the solid fraction dips below zero (see figure 5). Equation (5.2) indicates that this can only occur when the signs of ϕ and ϕ_z agree, which, in turn, can only occur after the ϕ-profile has developed an inflection point. Table 1 shows that the recirculation region must appear between the local minimum and the local maximum in the ϕ-profile. Comparing with figure 5, we see that these detailed relationships are observed in our computational results. These data correspond to a Rayleigh number of 12.72. By the the time the Rayleigh number drops to 12.70, the chimney has begun to form. The qualitative features of figure 5 were found to be robust upon refinement of the computational grid. The lower end of the recirculating region must coincide with the point where the chimney first appears, so that ϕ_z, ϕ and Q are all equal to zero at this point.

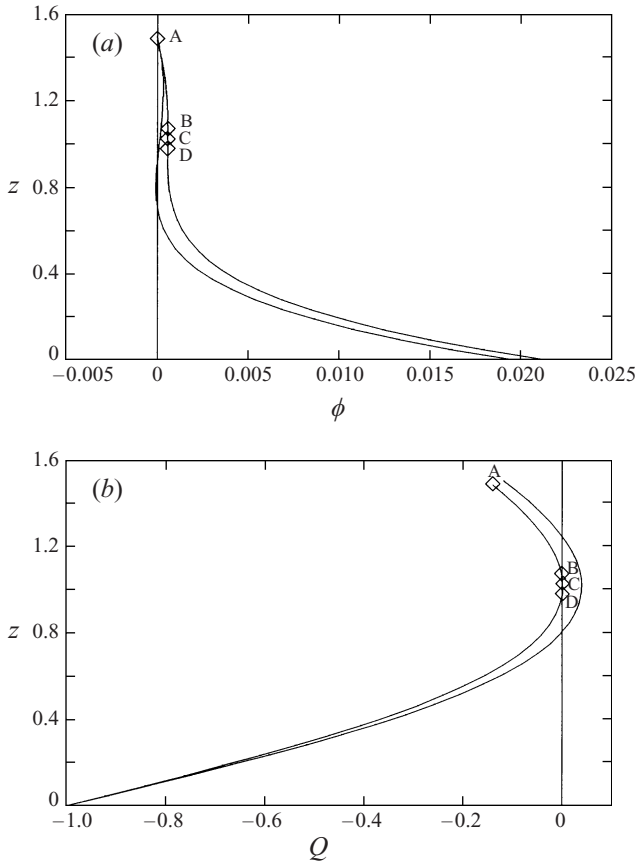

FIGURE 5. (*a*) The solid fraction ϕ as a function of z along the vertical symmetry line where chimneys first develop as the flow amplitude is increased. The labelled curve corresponds to $Ra = 12.72$ and marks the first net mass recirculation as the flow amplitude is increased. The labels correspond with the entries in table 1. The unlabelled curve corresponds to $Ra = 12.70$ and marks the conception of the chimney. (*b*) A similar plot for the total volume flux Q as a function of z. The remaining parameter values are the same as those in figure 2.

6. Discussion of liquid inclusions

The computations presented in the previous section are valid for solutions up to the point at which a liquid inclusion forms. The modelling and computation of solutions within and especially at the boundaries of the resulting liquid inclusions is somewhat more delicate. The essential difference between this case and the one modelled in § 2 is that, while flow always crosses a freezing interface moving from liquid to mush when there is no inclusion, it may cross either a freezing or dissolving interface in either direction when an inclusion is present. The purpose of this section is to clarify these issues and point out some qualitative features of the resulting flow. Presumably, fully developed chimneys grow out of liquid inclusions, and some of our conclusions can be extended to that case. It remains unclear, however, exactly how the change in topology from inclusion to chimney transpires.

Point	ϕ_z	ϕ	Q
A	$-$	0	$-$
B	0	$+$	$-$
C	$+$	$+$	0
D	0	$+$	$-$

TABLE 1. The letters A–D refer to the labelled points in figure 5(a, b), where one is able to see that one of the three quantities ϕ_z, ϕ or Q is equal to zero. The relationship between the sign of the remaining two quantities can be deduced from equation (5.2). Similar conclusions can be drawn for the unlabelled curves in figure 5(a, b).

Case	Flow direction	Boundary type	Unknowns	Boundary conditions
1	liquid $\rightarrow$ mush	freezing	h, ϕ	(6.2), (6.3)
2	liquid $\rightarrow$ mush	dissolving	h	(6.2)
3	mush $\rightarrow$ liquid	freezing	h, c, ϕ	(6.2), (6.1), (6.7)
4	mush $\rightarrow$ liquid	dissolving	h, c	(6.1), (6.2)

TABLE 2. The boundary conditions for mush–liquid interfaces when solutal diffusion is absent. As described in the text, these boundary conditions change depending on the direction of flow and whether the interface is freezing or dissolving.

6.1. *Boundary conditions relating concentration, solid fraction and interface position at mush–liquid interfaces*

In general the concentration, solid fraction and interface position at mush–liquid interfaces are determined by a combination of continuity and conservation of solute along with the assumption of local equilibrium at freezing interfaces. In the absence of solutal diffusivity, both the liquid and mushy regions are governed by hyperbolic solute-conservation equations. Within the liquid, the characteristics correspond to streamlines and concentration information is transported along with the flow. We can therefore prescribe continuity of concentration,

$$C = \theta, \tag{6.1}$$

whenever flow is from mush to liquid. Solute must be conserved at all boundaries, irrespective of the flow orientation. Allowing for discontinuities where flow enters the mush, this condition is expressed by

$$[C]_l^m \hat{\boldsymbol{n}} \cdot \boldsymbol{q} = \phi(\theta - \mathscr{C}), \tag{6.2}$$

where $\boldsymbol{q} = \boldsymbol{u} - \hat{\boldsymbol{k}}$ represents the total volumetric flux of fluid across the interface. Conditions expressing local equilibrium take different forms depending on the direction of flow and are described below, where we itemize which of these three boundary conditions applies to which type of interface. In total, there are four distinct cases that can be encountered. The boundary conditions that relate to solid fraction, concentration and local equilibrium in each of these cases are summarized in table 2 and illustrated in figure 6.

6.1.1. *Flow into mush along a freezing interface*

For a uniformly moving system that has reached steady state, a freezing interface is characterized by an upward pointing mush-to-liquid normal. The case where flow is from liquid to mush along such a boundary (inset 1, figure 6) is the simplest and most

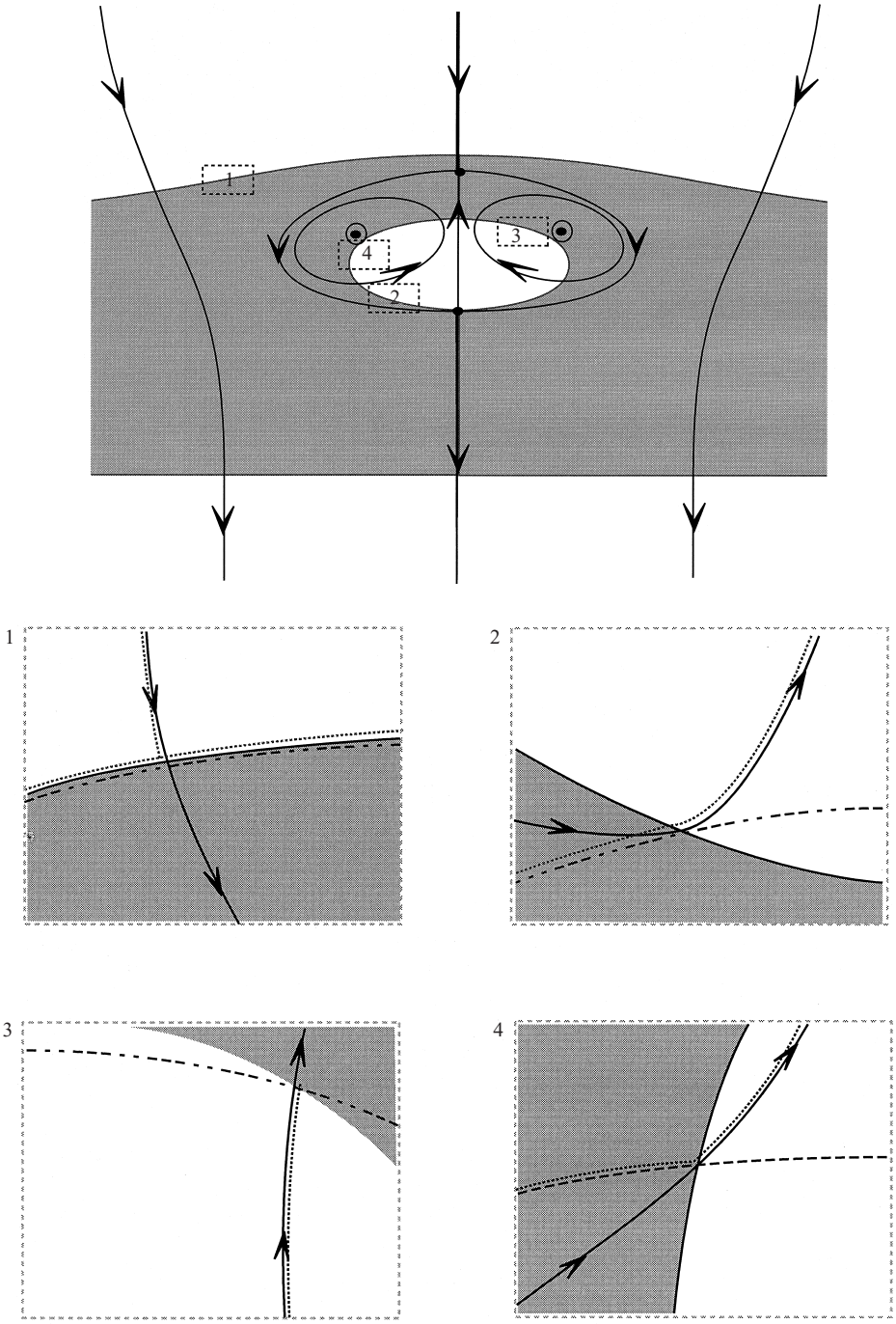

FIGURE 6. A sketch of a steady-state solution with a liquid inclusion and several representative streamlines. The four insets in this figure correspond to the four distinct boundary types identified in the text and itemized in table 2. The mush is indicated by the shaded region. Within the insets, contours with zero solid fraction are indicated with a solid line, isotherms with a dashed line, contours of solute concentration with a dotted line and streamlines with a solid line and arrows. The relationship between these various contours at these representative points can be deduced from the boundary conditions and governing equations. Notice that the streamline and isotherm in the second inset are tangent to one another at the mush–liquid interface.

thoroughly examined of the four types of interface. As noted earlier, the condition of local equilibrium is expressed by extending the liquidus relationship to the liquid side of the interface:

$$T|_l = C|_l. \tag{6.3}$$

Continuity of temperature together with (6.2) then implies $\phi = 0$.

6.1.2. *Flow into liquid along a freezing interface*

The type of interface shown in inset 2 of figure 6 forms the lower half of liquid inclusions. One would also expect to find this type of boundary along the wall of a fully developed chimney. Equations (6.2) and (6.3) combine once again to arrive at the condition $\phi = 0$. Unlike the previous case, we require a third independent condition for determining the interface position. Since we have deduced that the concentration is continuous across such a boundary, the liquidus relationship already applies on both sides of the interface and does not provide us with a new constraint. Instead, we arrive at a suitable condition by combining several weaker conditions. First, in keeping with the assumption of local equilibrium, we require

$$\boldsymbol{q} \cdot \nabla\theta \geqslant 0. \tag{6.4}$$

This tells us that the streamlines can only cross isotherms in the direction in which the temperature is increasing and follows from the fact that the concentration is fixed along a streamline after leaving the mush so that the temperature must only rise if the material is indeed a liquid. Secondly, we must have

$$\hat{\boldsymbol{n}} \cdot \nabla\phi \leqslant 0, \tag{6.5}$$

where the normal vector again points from mush to liquid. This condition follows from the fact that ϕ must be zero on interfaces where the flow passes from mush to liquid and that it cannot become negative. For steady-state solutions, we know that freezing boundaries have $\hat{\boldsymbol{n}} \cdot \hat{\boldsymbol{k}} \leqslant 0$, so that (6.5) implies

$$\phi_z \leqslant 0. \tag{6.6}$$

Finally, constraints (6.4) and (6.6) can be combined with equation (5.1) to give us

$$\boldsymbol{q} \cdot \nabla\theta = 0. \tag{6.7}$$

Here we have employed condition (2.7), so that the volumetric flux is continuous across the interface. Equation (6.7) then indicates that the flow must cross the interfaces parallel to the isotherms. This represents a new type of boundary condition and has been missing from earlier models that lack solutal diffusivity. This condition is made necessary by the fact that $\phi = 0$ can be derived from (6.2) on this type of boundary, so that it does not provide an independent constraint. Condition (6.7), or one analogous to it, is necessary to close any model of a fully developed chimney

6.1.3. *Flow into mush along a dissolving boundary*

The type of boundary featured in inset 3 of figure 6 might not arise in fully developed chimneys, but may be present in transient states and in steady states with liquid inclusions. The solid fraction can be determined at such a boundary by integrating (5.1), so that no local equilibrium condition is needed. Similarly, the concentration is already determined on both sides of the interface, the location of which must be determined by satisfying (6.2). Note that, unlike the other types of boundaries, ϕ and C are discontinuous at such an interface.

6.1.4. *Flow into liquid along a dissolving boundary*

Along the fourth type of boundary (inset 4, figure 6) the concentration is continuous so that (6.2) again reduces to $\phi = 0$. It is interesting to note that while no local equilibrium condition is necessary to resolve this free boundary, the constraint (6.4) must still be satisfied. The boundary is not over-constrained, however, since $\hat{\boldsymbol{n}} \cdot \hat{\boldsymbol{k}} \geqslant 0$, which reverses the inequality (6.6) and allows (5.1) to be satisfied for a range of non-negative heat fluxes.

6.2. *Some qualitative features of liquid inclusions*

One conclusion that can be deduced from these results is that the lower of the two stagnation points that bound the recirculating region of the flow always coincides with the lower boundary of a liquid inclusion after it has formed. This conclusion, which would seem to apply equally well to fully developed chimneys, follows from the fact that the streamline must be parallel to the isotherm at this point and that the isotherm must be horizontal (by symmetry). It can also be deduced that if the Rayleigh number can be adjusted so that there is a steady state with an inclusion that connects with the upper surface, the connection must occur when the upper boundary of the inclusion coincides with the upper stagnation point. This may provide a mechanism for chimney birth. We should note, however, that for a steady, fully developed chimney to exist the concentration of the effluent must be replenished to some extent before returning to the mush. One must imagine an idealized version of a chimney where solutal diffusion is ignored everywhere except in the far field, where mixing is assumed to occur. Under these assumptions, it appears that steady states with fully developed chimneys exist, but it is not clear how the topological transition from liquid inclusion to chimney is made.

Figure 7(*a*) shows a sketch of a steady-state solution with a liquid inclusion, several representative streamlines and selected isotherms. Figures 7(*b*) and 7(*c*) show idealized representations of the phase diagram with points that are labelled so that they correlate with the isotherms in figure 7(*a*). As a fluid parcel moves along a streamline, its thermodynamic state follows a path characterized by that shown in the phase diagrams, with figure 7(*b*) corresponding to any streamline that passes through the eutectic front and figure 7(*c*) corresponding to the streamline that bounds the recirculating region.

7. Summary

The present study improves upon earlier weakly nonlinear theories of convection in mushy layers by accurately modelling the shape of the mush–liquid interface and exhibiting solutions characteristic of the fully nonlinear regime. These computations provide evidence indicating that the mechanisms behind chimney formation are internal to the mushy layer and suggest that steady states with liquid inclusions within the mushy region may exist in parameter regimes with weakly viable chimneys.

The consideration of liquid inclusions naturally leads one to reconsider the boundary conditions at mush–liquid interfaces. In doing so we have formulated a new local equilibrium condition (6.7) that applies wherever there is flow from mush to liquid along a steadily freezing interface in idealized systems where diffusion has been neglected. Without such a condition it is impossible to model fully developed chimneys. An interesting consequence of this condition is that the lower boundary of a liquid inclusion or chimney must correspond to a stagnation point in

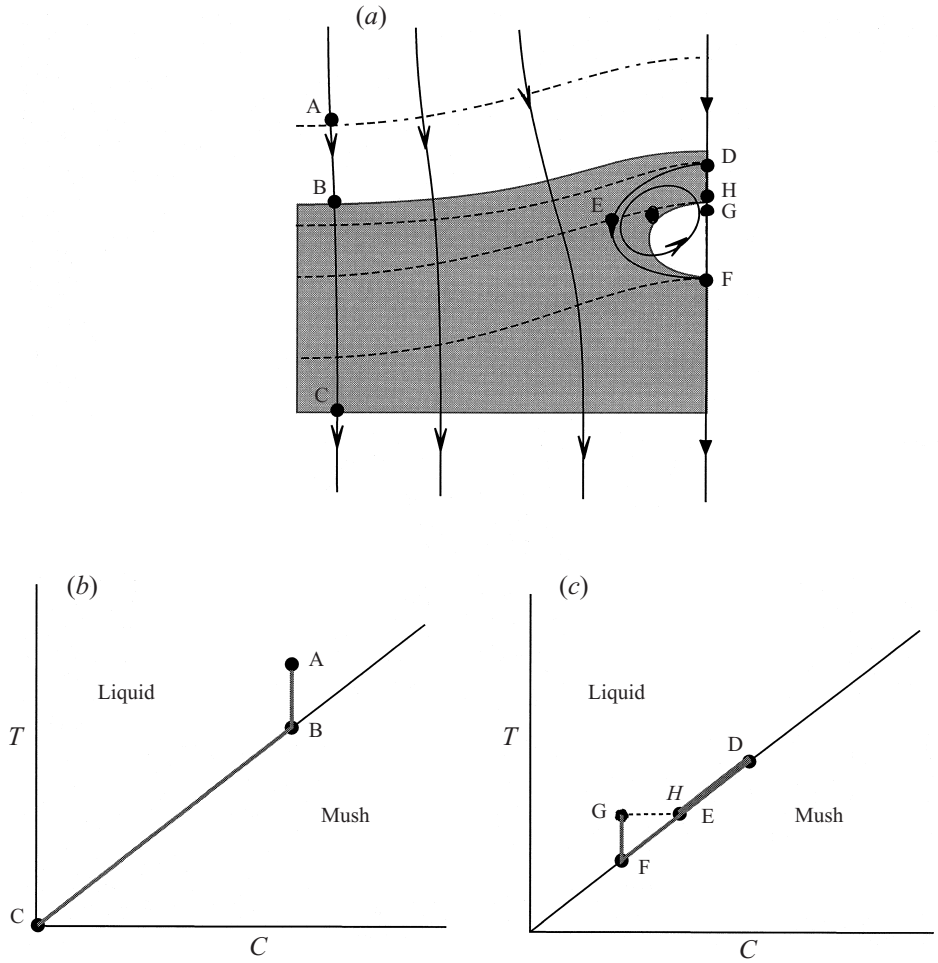

FIGURE 7. (*a*) A sketch of a steady-state solution with a liquid inclusion, several representative streamlines and selected isotherms. (*b*, *c*) Idealized representations of the phase diagram with points that are labelled so that they correlate with the isotherms in (*a*). As a fluid parcel moves along a streamline, its thermodynamic state follows a path characterized by that shown in the phase diagrams, with (*b*) corresponding to any streamline that passes through the eutectic front and (*c*) corresponding to the streamline that bounds the recirculating region. Note that the lower stagnation point bounding the recirculating region also marks the lower boundary of the inclusion.

the total volumetric flux when measured with respect to the steadily moving solid phase.

Convection in real mushy layers is complicated and time-dependent for a variety of reasons, including instabilities in the plume and finite domain size. The study of steady states is a tool for understanding the dominant mechanisms of these dynamics. Future work needs to address both the computational and modelling difficulties associated with topological changes that take place in temporally evolving mushy layers.

The authors would like to acknowledge support by the NSF-NATO postdoctoral fellowship program (T. P. S.) and the Natural Environment Research Council (M. G. W.).

REFERENCES

Amberg, G. & Homsy, G. M. 1993 Nonlinear analysis of buoyant convection in binary solidification with application to channel formation. *J. Fluid Mech.* **252**, 79–98.

Anderson, D. M. & Worster, M. G. 1995*a* Weakly nonlinear analysis of convection in mushy layers during the solidification of binary alloys *J. Fluid Mech.* **302**, 307–331.

Anderson, D. M. & Worster, M. G. 1995*b* A new oscillatory instability in a mushy layer during the solidification of binary alloys. *J. Fluid Mech.* **307**, 245–267.

Beavers, G. S. & Joseph, D. D. 1967 Boundary conditions at a naturally permeable wall. *J. Fluid Mech.* **30**, 197–207.

Beckermann, C. & Wang, C. Y. 1995 Multiphase/scale modeling of alloy solidification. *Ann. Rev. Heat Transfer* **6**, 115–198.

Bergman, M. I. & Fearn, D. R. 1994 Chimneys on the Earth's inner-outer core boundary? *Geophys. Res. Lett.* **21**, 477–480.

Chen, F., Lu, J. W. & Yang, T. L. 1994 Convective instability in ammonium chloride solution directionally solidified from below. *J. Fluid Mech.* **276**, 163–187.

Coriell, S. R. & McFadden, G. B. 1993 Morphological stability. In *Handbook of Crystal Growth*, Vol. 1 (ed. D. T. J. Hurle), pp. 785–857. North-Holland.

Eide, L. I. & Martin, S. 1975 The formation of brine drainage features in young sea ice. *J. Glaciology* **14**, 137–154.

Emms, P. W. 1998 Freckle formation in a solidifying binary alloy. *J. Engng Maths* **33**, 175–200.

Emms, P. W. & Fowler, A. C. 1994 Compositional convection in the solidification of binary alloys. *J. Fluid Mech.* **262**, 111–139.

Fearn, D. R., Loper, D. E. & Roberts, P. H. 1981 Structure of the Earth's inner core. *Nature* **292**, 232–233.

Flemings, M. C. 1974 *Solidification Processing*. McGraw Hill.

Flemings, M. C. & Nereo, G. E. 1967 Macrosegregation, Part I. *Trans. Metall. Soc. AIME* **239**, 1449–1461.

Flemings, M. C. & Nereo, G. E. 1968 Macrosegregation, Part III. *Trans. Metall. Soc. AIME* **242**, 50–55.

Fowler, A. C. 1985 The formation of freckles in binary alloys. *IMA J. Appl. Maths* **35**, 159–174.

Hellawell, A., Sarazin, J. R. & Steube, R. S. 1993 Channel convection in partly solidified systems. *Phil. Trans. R. Soc. Lond.* A **345**, 507–544.

Hills, R. N., Loper, D. E. & Roberts, P. H. 1983 A thermodynamically consistent model of a mushy zone. *Q. J. Mech. Appl. Maths* **36**, 505–539.

Press, W. H., Teukoisky, S. A., Vettering, W. T. & Flannery, B. P. 1992 *Numerical Recipes*. Cambridge University Press.

Roberts, P. H. & Loper, D. E. 1983 Towards a theory of the structure and evolution of a dendrite layer. In *Stellar and Planetary Magnetism* (ed. A. M. Soward), pp. 329–349. Gordon & Breach.

Schulze, T. P. & Worster, M. G. 1998 A numerical investigation of steady convection in mushy layers during the directional solidification of binary alloys. *J. Fluid Mech.* **356**, 199–220.

Tait, S. & Jaupart, C. 1992 Compositional convection in a reactive crystalline mush and melt differentiation. *J. Geophys. Res.* **97**, 6735–6756.

Worster, M. G. 1986 Solidification of an alloy from a cooled boundary. *J. Fluid Mech.* **167**, 481–501.

Worster, M. G. 1991 Natural convection in a mushy layer. *J. Fluid Mech.* **224**, 335–359.

Worster, M. G. 1992 Instabilities of the liquid and mushy regions during solidification of alloys. *J. Fluid Mech.* **237**, 649–669.

Worster, M. G. 1997 Convection in mushy layers. *Ann. Rev. Fluid Mech.* **29**, 91–122.